

C-Scan Imaging for Bond Testing Inspection

René Sicard, Nicolas Grimard and Sam Serhan*

*TecScan Systems Inc.
75, boul. De Mortagne, Suite 122
Boucherville (Québec) Canada
J4B 6Y4
Tel. : 1-450-641-5876
Fax. : 1-450-641-5873*

www.tecscan.ca

**Corresponding author: Rene.Sicard@tecscan.ca*

Abstract

In today's manufacturing world, the use of adhesive-bonded components is growing, especially in the aerospace industry. Such an increase adds more demands for reliable NDT inspections of those components to ensure the quality of the end product. C-Scan imaging have been widely used for the detection and sizing of indications in most conventional UT applications, providing more intuitive analysis schemes. However, similar imaging has not been widely used for bond testing.

In this work, the evaluation of the advantages of performing C-Scan imaging out of specialized bond testing techniques is being addressed. Bond testing inspections are performed using off-the-shelf equipment while C-Scan type imaging is performed in order to assess the added value for the detection, sizing and positioning of flaws. Tests were carried out using the resonance mode of a bond tester coupled with an acquisition and analysis software designed for bond testing. Results point to the advantages of bond testing C-Scan imaging over current bond testing practice.

1. Introduction

Adhesive-bonded components are widely used in the aerospace industry, therefore requiring reliable NDT inspection technologies and methods to ensure the quality of these parts. While conventional ultrasonic and guided waves have been used for the inspection of bonds for quite some time, the development of advanced and dedicated technologies lead to the development by some manufacturers of bond testing instruments which all use specialized analysis techniques that proved to be adequate for the detection of bonding defects. Most bond testing equipment manufacturers propose hand-held system where probe motion is controlled manually by an operator. While this methodology typically allows for detection of unbounded type of defects using alarms, it does not systematically provide accurate defect sizing, positional information, or record complete data for reference or additional analysis.

C-Scan imaging and display have been widely used for the detection and sizing of indications in most conventional UT applications. However, very few equipment manufacturers propose C-Scan imaging capabilities for bond testing, which would allow for more intuitive and accurate analysis possibilities in terms of detection, sizing and positioning.

In this paper, we present results obtained with a C-Scan imaging software developed to complement bond testing equipments. With the help of two generic samples, advantages of performing C-Scan imaging is highlighted.

2. Background : Specialized Bond Testing Technologies

Three main technologies have been integrated and used in commercially available bond testing instruments:

- Resonance
- MIA (Mechanical impedance Analysis)
- Pitch-and-Catch

While all three techniques make use of sounds or ultrasounds, their mode of operation is different. The following is a short review of each technique.

(a) Resonance mode

In resonance mode, a highly resonant, narrowband transducer is excited at its resonance frequency with a tuned continuous wave. This method requires an ultrasonic coupling between the transducer and the tested part (low-viscosity coupling material). The frequency of the probe is selected to optimize the generation of standing waves inside the tested part.

The mode of operation of the resonance mode is then similar to an eddy current inspection. The impedance of the probe is monitored on an impedance plane (horizontal and vertical components). The acoustic impedance of the tested part changes the resonance characteristics of the probe, which allows to monitor the effects of the part by changes of the probe impedance characteristics at the resonance frequency. Since the thickness of the part influences the acoustic impedance, relative measurements are made between a known reference (or good section of the part) and the rest of the part. The signal is therefore nulled by placing the probe on an area that is free from defects. Changes in the signal amplitude and phase are then representative of thickness changes caused by the presence of disbonds, delaminations, thinner parts, etc. Most of the time, the phase angle can be used as an indicator of depth of the defects.

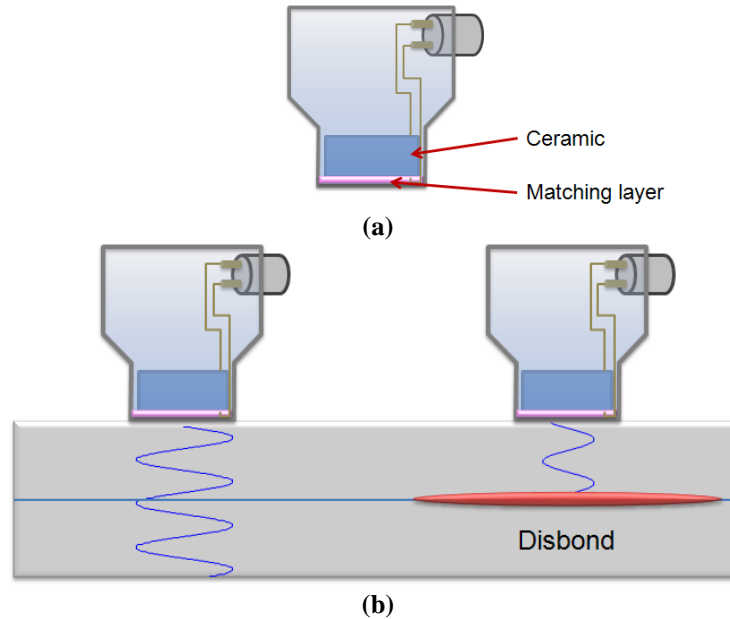


Fig. 1. Graphical representation of a resonance probe. (a) Internal conception; (b) Representation on top of a bonded sample – wave resonance characteristics are influenced by the presence of the disbond.

(b) MIA mode

Signal monitored by MIA probes are typically of the same nature of the resonance probe, i.e. represented on an impedance plane, although it does not rely on measuring changes in the resonance characteristics of the probe. A MIA probe is composed of a driving and receiving elements, where only the receiving element is in contact with the material under test (figure 2). Waves are sent from the driving to the receiving. The loading of the receiving element is affected by the stiffness of the tested part that is in contact with. The presence of a disbond affects the local stiffness of the material and its presence can be monitored by changes in the impedance of the receiver. Again, the probe is nulled and relative measurements can be made between a reference sample or defect-free area and the rest of the part.

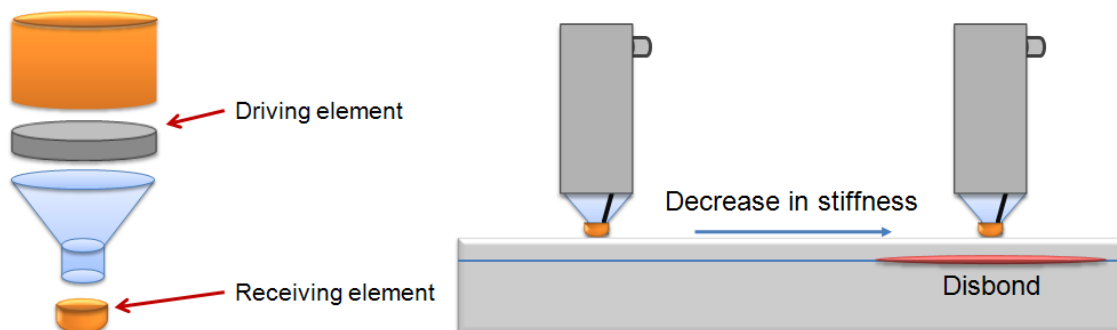


Fig. 2. Graphical representation of a MIA probe. (a) Internal conception; (b) Representation on top of a bonded sample – stiffness of the material is affected by the presence of a disbond and monitored by the receiving tip of the probe.

(c) Pitch-and-Catch

The pitch-and-catch mode makes use of local changes occurring in the tested part in the presence of defects. In the presence of a disbond or delamination, the loss of mechanical coupling at the defect location results in a local behavior that can be associated to two plates placed one on top of the other, where the original thickness of the sample is divided into a layer on top and a layer below the defect. Under certain conditions, waves propagating in the plane of a plate are called guided plate waves or Lamb waves.

Two of the main characteristics of Lamb waves is that they have multiple modes of propagation and that their velocity changes with frequency and thickness of the plate (figure 3). By sending guided waves in the sample, different plate thickness conditions caused by the presence of defects can therefore be monitored.

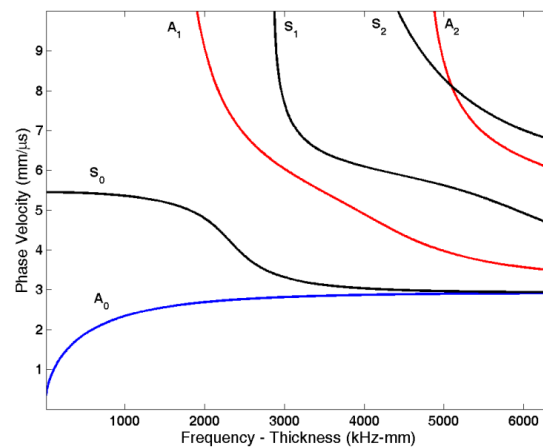


Fig. 3. Example of dispersion curves of the phase velocity of Lamb waves in an aluminum plate.

Pitch-and-catch transducers used in bond testing don't need couplant and are composed of an emitter and a receiver element that are both in contact with the tested material (figure 4a). Low frequency waves are sent in the material received by the receiving element. In the presence of a disbond, a local change in material thickness can be monitored by the resulting different guided wave behavior.

This technique is known to predominantly generate flexural waves, resulting in the fundamental Lamb mode A_0 , which phase velocity varies sharply with thickness at low frequencies (figure 4b).

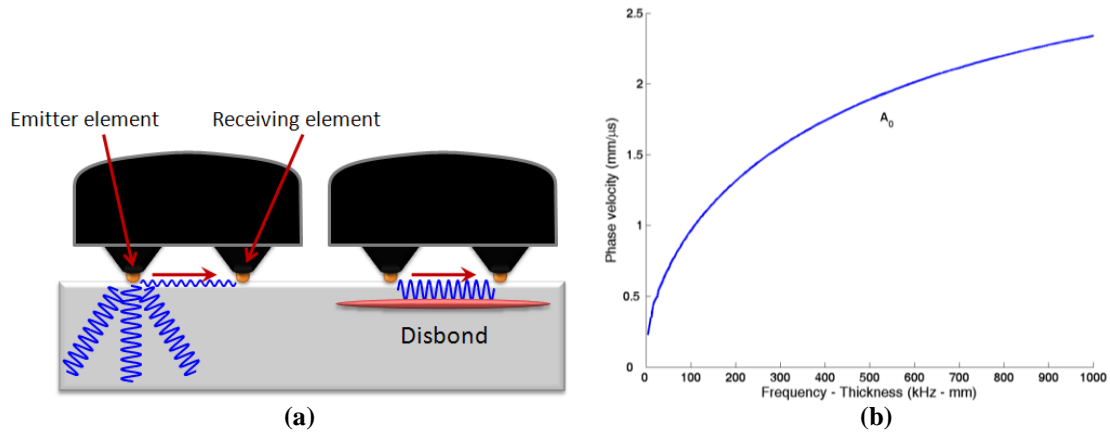


Fig. 4. Graphical representation of a pitch-and-catch probe. The presence or absence of a disbond affect the behavior of the guided waves propagating from the emitter to the receiver tip. (b) Phase velocity dispersion curve of the A_0 Lamb wave mode in an aluminum plate.

Changes in amplitude and phase of a single or multiple swept frequencies as well as amplitude changes of a RF signal can be monitored to detect disbonds in pitch-and-catch mode. The main difference between this mode of operation and the resonance and MIA modes is that it doesn't involve continuous waves, but rather tone bursts. A pulse repetition frequency is therefore associated with the pitch-and-catch mode.

3. Experimental setup

Two samples were inspected for this study. The first sample is an 8 plies, $0^\circ/90^\circ$ carbon/epoxy sample with a thickness of 1.9 mm and containing rectangular Teflon® inserts to simulate internal delaminations. A conventional ultrasonic C-Scan inspection was performed on the sample prior to the tests with the bond testing equipment as a reference (figure 5).

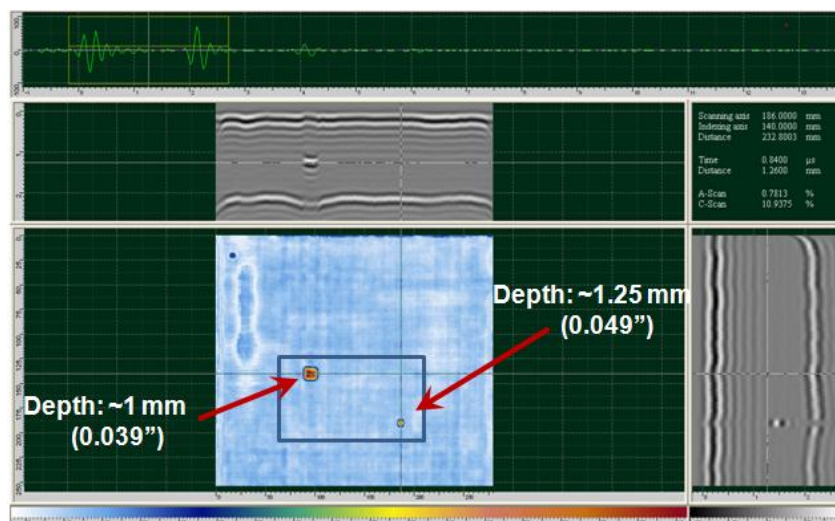


Fig. 5. C-Scan image obtained on sample 1 with a 10MHz, 0.25" flat transducer (screenshot from TecView™ UT). The rectangle on top of the C-Scan view indicates the area scanned with the resonance probe.

The second sample is an aerospace bonding standard composed of an aluminum honeycomb core and external layers of carbon/epoxy composite material (figure 6).

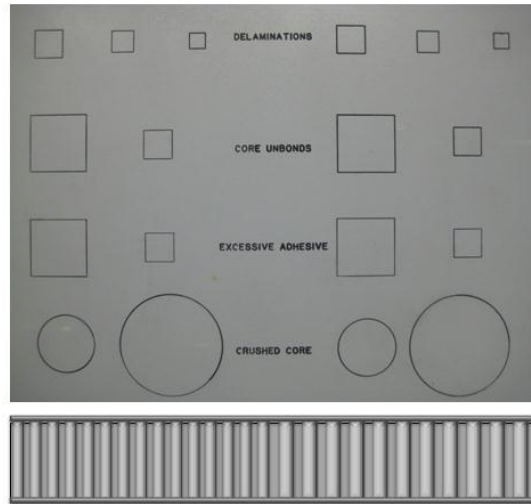


Fig. 6. Picture of the aerospace standard sample for bond defects (top) and a representation of its internal structure (bottom). Core size is 0.187" on the left half and 0.250" on the right half.

All of the inspections presented in this paper were performed using resonance probes. The scans were performed using the ARMANDA automated XY scanner powered by the commercial software TECVIEW™ BT dedicated to C-Scan imaging and analysis for bond testing. A BondMaster 1000e+ from Olympus NDT was used for the bond testing measurements and inspection data were recorded using a 14-bit digitizer (figure 6).



Fig. 6. Experimental setup: ARMANDA scanner, TecView™ BT software, BondMaster 1000e+ and a 14-bit digitizer.

4. Results and Discussion

This section describes the experiments conducted during the course of this work.

a) FIRST SAMPLE: TEFLON® INSERTS IN A CARBON/EPOXY PLATE

The inspection of sample 1 was performed using a 250 kHz resonance transducer with a resolution of 1 mm x 1 mm (0.039" x 0.039"). As a reference, the C-Scan section obtained with conventional UT (10 MHz) and corresponding to the area covered by the resonance probe is shown in figure 7.



Fig. 7. C-Scan obtained using a conventional 10MHz transducer in pulse-echo mode: approximate area corresponding to the section covered by the resonance probe.

The result from the C-scan inspection performed using the resonance probe is shown in figure 8 and is very similar to the result obtained with conventional UT. Since the data of the resonance mode is presented in the form of impedance readings (two components), four choices of displays were available: absolute amplitude (option selected for figure 8), horizontal component, vertical component and phase angle.

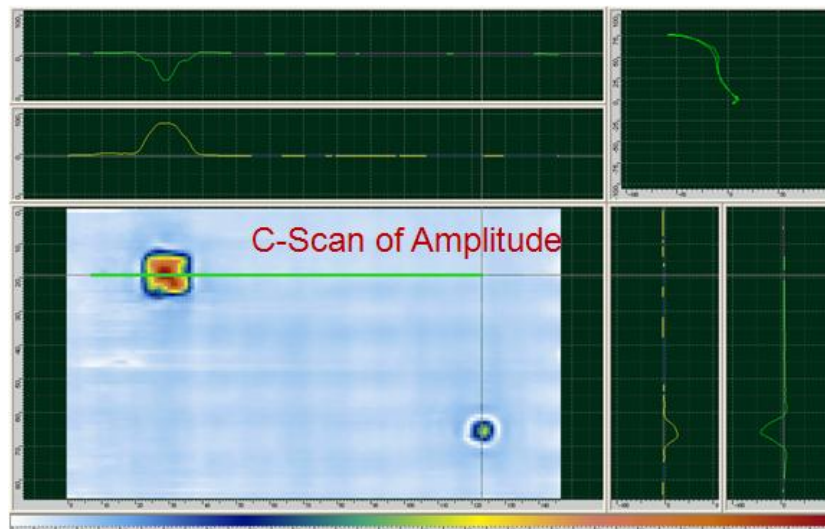


Fig. 8. C-Scan obtained using a 250 kHz resonance probe using the BondMaster 1000e+ and recorded and displayed by TecView™ BT.

Sizing (-6dB drop method) was performed on the C-Scan obtained from resonance bond testing mode as well as from the conventional pulse-echo ultrasonic inspection for

comparison. Results from this sizing are presented in Table 1 and show that similar dimensions are obtained with the 250 kHz resonance probe and the conventional 10 MHz pulse-echo probe. This conclusion points to a probable equivalent sizing capabilities between both methods, i.e. using C-Scan imaging with bond testing can provide sizing capabilities equivalent to conventional pulse-echo imaging.

Table 1. Comparison of the -6dB drop sizing obtained on the pulse-echo scan (10 MHz) and the resonance mode scan (250 kHz).

	Insert 1 X	Insert 1 Y	Insert 2 X	Insert 2 Y
UT – 10 MHz	13 ± 1 mm	12 ± 1 mm	6 ± 1 mm	7 ± 1 mm
BT – 250 kHz	11 ± 1 mm	11 ± 1 mm	6 ± 1 mm	6 ± 1 mm

An interesting option offered by the impedance plot format is the possibility to draw C-Scans using the phase angle. Since this value can most of the time be related to the depth of defects, it can provide a defect depth mapping of the sample. As an example, the C-Scan of time-of-flight calculated from the 10 MHz pulse-echo inspection is presented in figure 9 for reference, while the phase angle C-Scan is shown in figure 10a and figure 10b. In the latter case, a grayscale colormap is used to draw the phase angle C-Scan. Alarms corresponding to specific phase angle ranges were applied to the data set and the coordinates on the C-Scan where the alarms are triggered were color coded to represent alarm detection. In both cases, a notable difference can be observed between the color coding of inserts 1 and 2. This indicates that with a proper calibration, direct readings of defect depth could be done on the C-Scan.



Fig. 9. Time-of-flight C-Scan calculated from the 10 MHz pulse-echo inspection data..

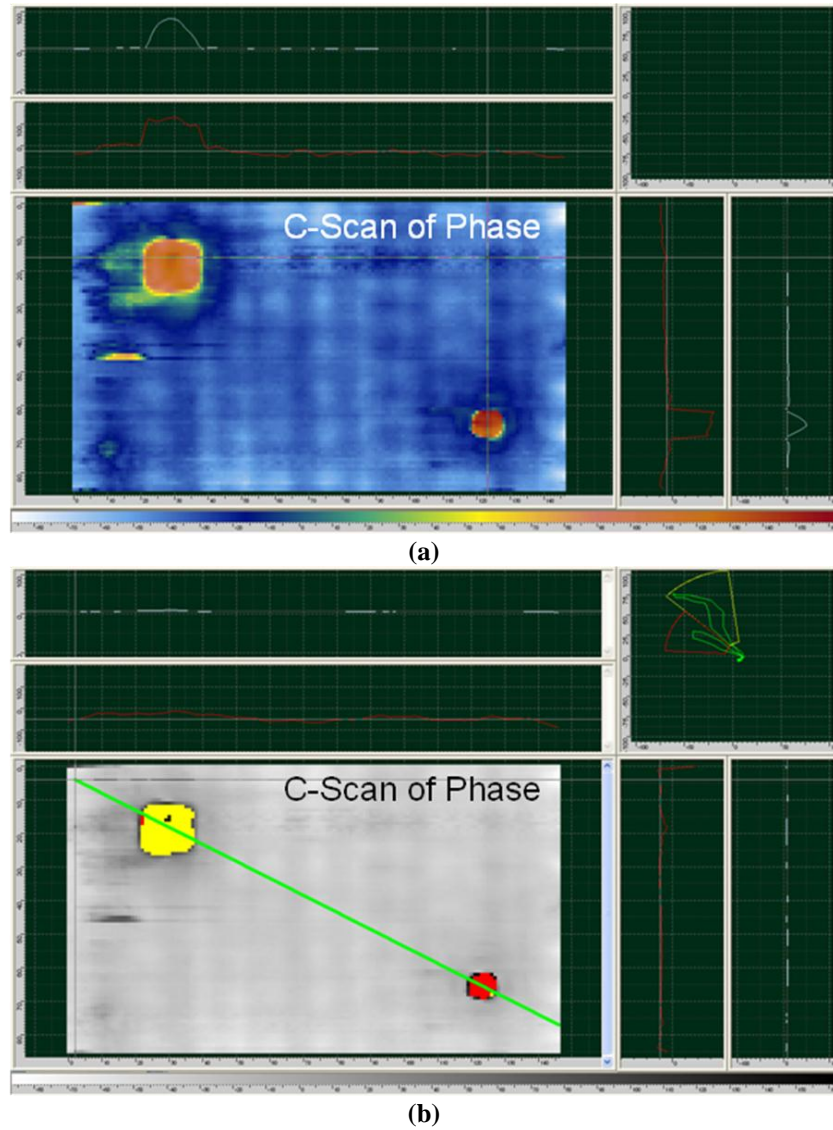


Fig. 10. C-Scan obtained from the phase angle values of the same data set as figure 8 (sample 1). (a) Rainbow colormap ; (b) Grayscale colormap with triggered alarms information color coded on top of the C-Scan image.

b) SECOND SAMPLE: AEROSCAPE BOND DEFECTS STANDARD

The inspection of sample 2 was performed using a 110 kHz resonance transducer with a resolution of 1 mm x 1 mm (0.039" x 0.039"). The absolute amplitude C-Scan resulting from this inspection is shown in figure 11. This result shows that one of the four defect types present in the sample (core unbonds – second rows of defects) is not detected with a high signal-to-noise ratio. In fact, only the contour of the sample appear to be visible from the absolute amplitude C-Scan image. Plus, parts of the crushed cores area are also not detected with a high SNR (last row of circular defects).

Figure 12 shows the C-Scan of the phase angle of the same data set, which provides a different view of the internal structure; the phase angle of the signal clearly identifies the areas corresponding to core unbonds and crushed cores as well as the missing areas of the crushed cores defects. This result represents a perfect example of the benefits of using C-Scan imaging with bond testing data; the repetitive behavior of a measurable value (phase angle) within a definable area represents a valuable indication of an internal structural change in the material.

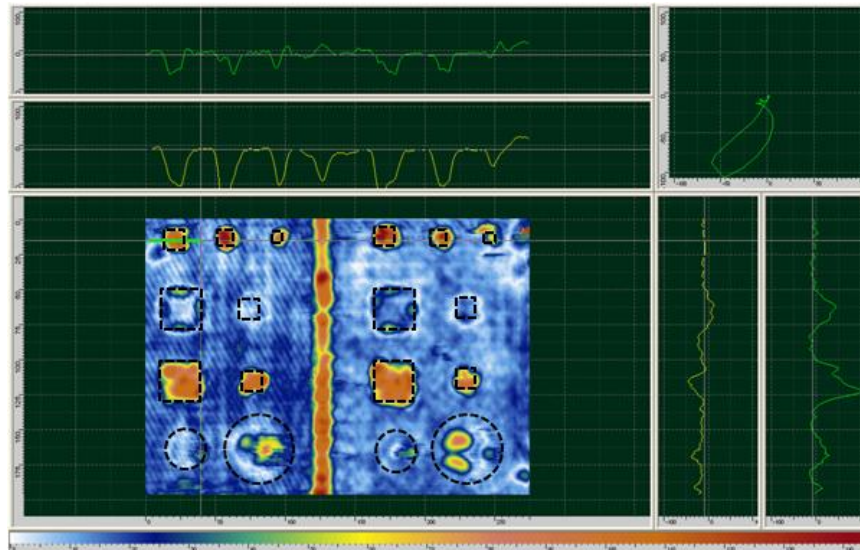


Fig. 11. C-Scan obtained from the absolute amplitude of the resonance mode inspection (110 kHz) of sample 2.

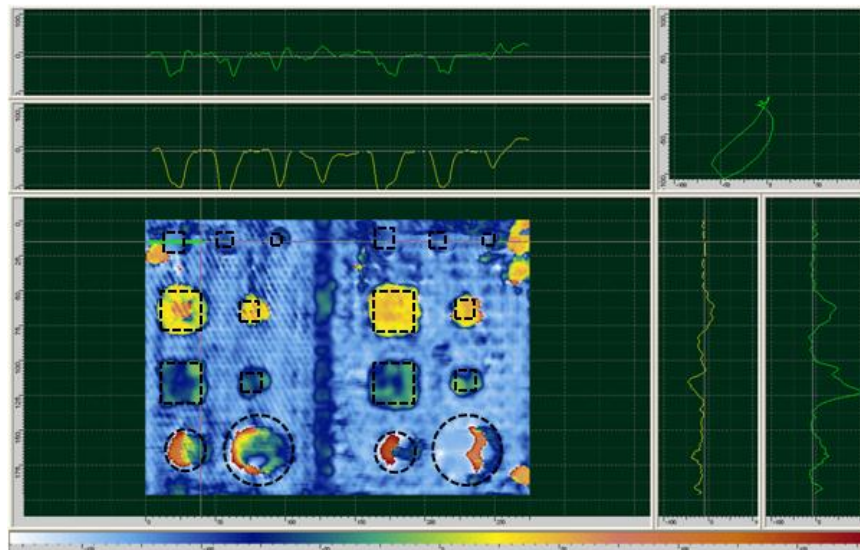


Fig. 12. C-Scan obtained from the phase angle (sample 2).

Finally, the additional analysis possibilities offered by C-Scan capabilities allow for the optimization of the results with the use of post-processing nulling and rotations. As an example, the absolute amplitude C-Scan obtained from the inspection of sample 2 is calculated for different nulling possibilities. Figure 13 shows the C-Scan obtained from

the original data recorded following a live null on a randomly selected area of the sample. The enlarged view of the impedance plot window displayed beside the C-Scan shows the impedance plot corresponding to a defect-free area of the C-Scan (green line drawn on the C-Scan image). This enlarged view points to a bad selection of the nulling position.

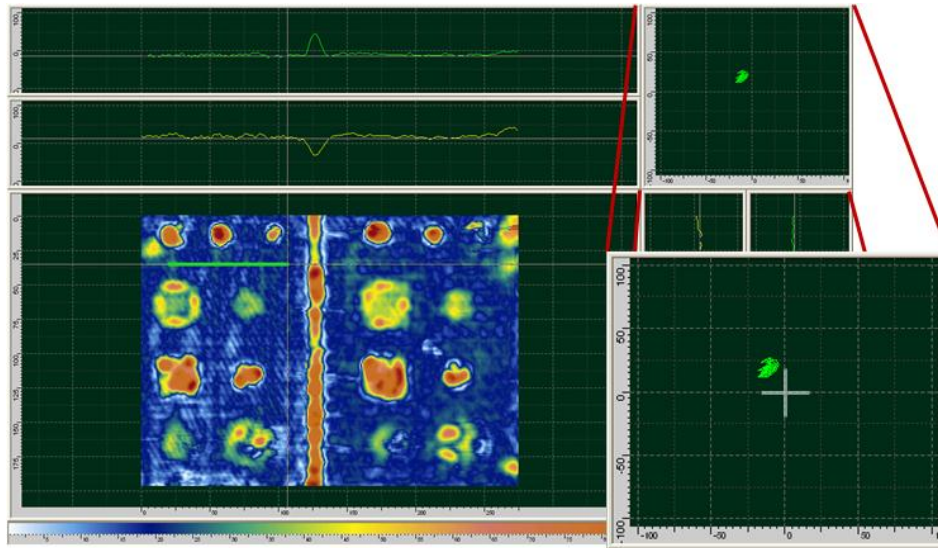


Fig. 13. C-Scan obtained from the absolute amplitude signal after a live nulling operation performed prior to the scan.

A post-processing nulling was performed on the C-Scan by subtracting the signal recorded at a selected defect-free location. This post-nulling operation was performed at a few locations until an optimal signal-to-noise was achieved. The C-Scan absolute amplitude C-Scan resulting from this post-nulling is displayed in figure 14. The enlarged impedance plot view of a defect-free area (same as figure 13) shows that this post-nulling operation improved the results by bringing the defect-free areas response closer to zero.

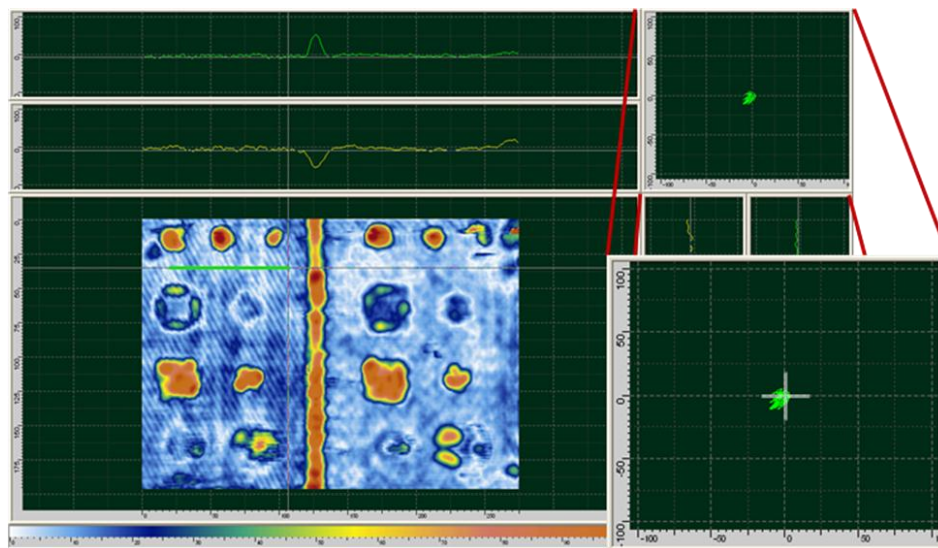


Fig. 14. C-Scan obtained from the absolute amplitude signal after a post-processing nulling operation performed on a selected location in the recorded C-Scan.

An additional nulling option offered by post-processing of the data is the line reference subtraction; if a repeatable natural structural feature masks the response from defects, a set of null locations can be selected to remove or minimize the structural response from the C-Scan. As an example, the separator between the 0.187" and 0.250" cores (vertical line in the center of the C-Scans of sample 2) is minimized in figure 15 following a horizontal line nulling performed at the position indicated by arrows. Again, the enlarged impedance plot of a selected defect-free area shows a response that remains around zero after post-processing nulling.

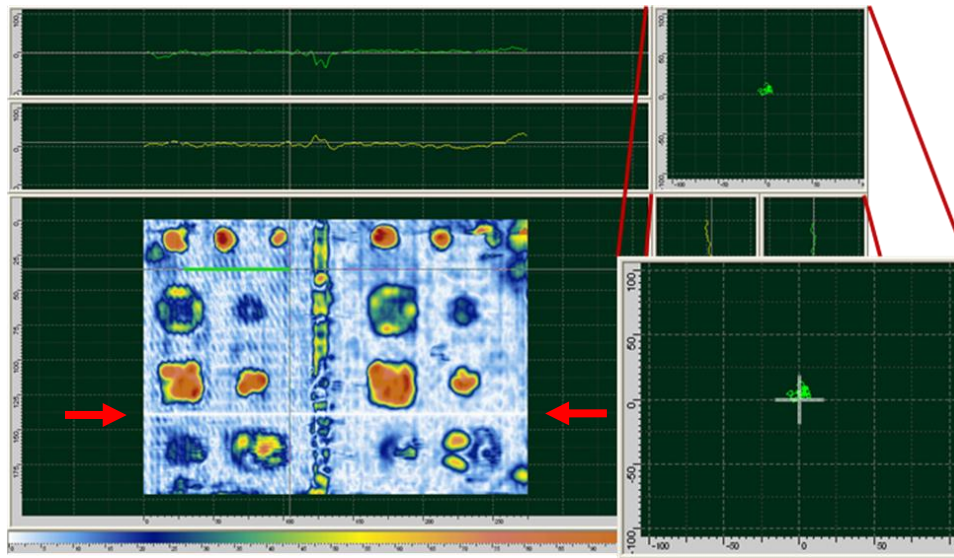


Fig. 15. C-Scan obtained from the absolute amplitude signal after a post-processing nulling operation performed on a selected location in the recorded C-Scan.

5. Conclusion

In this paper, we have shown that C-Scan imaging can provide useful additional data that can complement specialized bond testing. By recording the output signal of a bond testing instrument to perform C-Scan imaging, additional analysis options are made available to inspectors in terms of defect sizing and recognition capabilities. Plus, C-scan imaging provides an intuitive representation of the inspection data that allows recognizing geometrical patterns within multiple readings.

The study of a resonance inspection of a carbon/epoxy composite plate allowed highlighting the defect sizing capabilities, which proved to be equivalent to that of 10MHz conventional pulse echo scanning. Plus, C-Scan representing the phase angle of the signal displayed image contrast that was representative of the different depths of the Teflon® inserts that were detected. The ability to display C-Scans based on triggered alarm information was also highlighted in the same context; alarms selected to detect specific phase angle ranges can be used to map defects depth.

The analysis of an aerospace bond defect standard also help to identify the advantages of adding C-Scan imaging capabilities to specialized bond testing techniques. Phase angle C-Scan information was used to enhance the detection of defects that were difficult to detect by solely relying on signal amplitude information (unbond and crushed cores). The analysis of this sample also allowed to demonstrate how simple post-processing nulling operations could be used to optimize inspections by correcting a possible bad choice of live nulling location.